# Magnetization reversal in circularly exchange-biased ferromagnetic disks

M. Tanase,[1] A. K. Petford-Long,[1] O. Heinonen,[2] K. S. Buchanan,[3,*] J. Sort,[4] and J. Nogués[5]
[1]*Materials Science Division, Argonne National Laboratory, 9700 S Cass Avenue, Lemont, Illinois 60439, USA*
[2]*Recording Heads Operation, Seagate Technology, 7801 Computer Avenue, Bloomington, Minnesota 55435, USA*
[3]*Center for Nanoscale Materials, Argonne National Laboratory, 9700 S Cass Avenue, Lemont, Illinois 60439, USA*
[4]*Institució Catalana de Recerca i Estudis Avançats (ICREA) and Departament de Física, Universitat Autònoma de Barcelona, 08193 Bellaterra, Spain*
[5]*Institució Catalana de Recerca i Estudis Avançats (ICREA) and Centre d'Investigació en Nanociència i Nanotecnologia (ICN-CSIC), Campus Universitat Autònoma de Barcelona, 08193 Bellaterra, Spain*
(Received 24 September 2008; published 27 January 2009; corrected 6 February 2009)

We investigate the reversal behavior of circularly exchange-biased micron-sized bilayer disks of Permalloy (Py)/IrMn and CoFe/IrMn. A circular exchange bias is induced by imprinting the vortex configuration of the ferromagnetic layer into the IrMn when the disks are cooled in zero external field through the blocking temperature of IrMn. The resulting circular exchange bias has a profound effect on the reversal behavior of the ferromagnetic magnetization. In Py/IrMn disks the reversal takes place via vortex motion only, and the behavior is controlled by the exchange bias; it is reversible over a range of small fields and the vortex maintains a single chirality throughout reversal, determined by the chirality of the exchange bias. In CoFe/IrMn disks the non-negligible magnetocrystalline anisotropy causes a reversal via both vortices and domain walls resulting in a finite coercivity, and the behavior is controlled by microstructure. We verify that circular exchange bias does not give rise to a hysteresis loop shift. It lowers coercivity with respect to the field-cooled case, and in Py/IrMn disks it even causes completely reversible magnetic behavior. In both Py/IrMn and CoFe/IrMn disks, circular exchange bias removes the randomness (i.e., stochastic processes due to thermal activation) inherent in single-layer ferromagnetic disks and causes the magnetic behavior to be reproducible over time.

DOI: 10.1103/PhysRevB.79.014436 PACS number(s): 75.60.Jk, 85.70.Kh, 75.75.+a, 85.75.Dd

## I. INTRODUCTION

Ferromagnetic (FM) nanostructures supporting vortex magnetization[1] are of considerable interest because of their fundamental properties and because of their potential applications in ultrahigh-density recording media,[2] magnetic random access memories,[3,4] and spintronic logic devices.[5] Magnetic vortices carry information in their chirality and polarity[6,7] each having two possible orientations. Thus, they have four different magnetic states rather than the conventional two magnetic states of other ferromagnetic nanostructures. Methods to control the chirality in single FM layer elements exploit an asymmetry either in the element shape[8–12] or in the applied field, such as using a magnetic force microscopy (MFM) tip,[13] magnetic pulses,[14] or a magnetic field gradient,[15] as well as the magnetization history.[16] More recently exchange bias (EB) has been explored in combination with a homogeneous external field to control reversal in Co/IrMn elliptical dots[17] and rings.[18] A combination of spin torque and Oersted field has been used to switch the chirality in pseudospin valve rings[19] and the spin torque effect alone has been predicted to switch the chirality in vortex-supporting spin-valve disks.[20]

EB (Ref. 21) obtained by cooling the antiferromagnet/ferromagnet (AF/FM) bilayer in a saturating field through the blocking temperature of the AF has been extensively studied in both continuous thin films[22–24] and nanostructures.[25] EB can add an extra mechanism by which the reversal behavior of the FM vortex can be controlled. EB patterned magnetic elements have been shown to support FM vortex structures with shifted constricted loops,[26–28] and the EB effect was reported to pin the circulating direction of magnetization in Permalloy (Py)/IrMn/Py asymmetric rings after the application of saturating fields.[29] Recently it has been proposed that exchange bias itself can take on a vortex-like or circular configuration by zero-field cooling (ZFC) patterned Py/IrMn micron-sized disks exhibiting vortex magnetization through the blocking temperature of the antiferromagnet. The FM vortex field becomes "imprinted" into the AF resulting in exchange bias with circular symmetry.[30,31] This results in an enhanced stability of the vortex state over a wider applied field range and a reversible central part of the hysteresis loop. Unlike conventional exchange bias obtained by cooling in external fields, the ZFC treatment does not result in a macroscopic hysteresis loop shift. A displaced vortex state can be maintained at remanence by reducing the strength of the magnetic field applied during the cooling procedure. Magnetization reversal via vortex formation is observed even upon cooling in saturating fields, but a critical angle appears between the applied and the exchange bias field, beyond which vortex reversal is replaced by coherent rotation.[26] The circular exchange bias geometry provides a low-energy vortex reference state, which has been shown via micromagnetic modeling to control the magnetization dynamics (vortex core precession and spin-wave dynamics) of NiFe/IrMn disks.[32] In this paper the magnetization reversal in micron-sized disks of CoFe and Py, both as single FM layers and exchange biased to 5 nm of IrMn, has been investigated using Lorentz microscopy, micromagnetic simulations and magneto-optical Kerr magnetometry (MOKE). This combination of techniques[33,34] allows us to address both the collective behavior of arrays of disks and the behavior of individual disks and to make a quantitative determination of

 

the exchange bias field in circular geometry characterized by the absence of a macroscopic loop shift. In addition to confirming the previous findings, we show that circular exchange bias leads to a different type of magnetization reversal.

## II. EXPERIMENTAL

Arrays of $20\times20$ 1 $\mu$m diameter disks with a periodicity of 2 $\mu$m were fabricated by electron-beam lithography and lift-off on commercial 300-$\mu$m-thick Si wafers coated with a 50-nm-thick SiN layer. Four different configurations were deposited: single FM layers consisting of //Ta/$Ni_{80}Fe_{20}$/Cr(5/12/2 nm) or //Cr/$Co_{90}Fe_{10}$/Cr(2/10/2 nm) and bilayers of //Ta/$Ni_{80}Fe_{20}$/IrMn/Cr(5/12/5/2 nm) and //Cr/$Co_{90}Fe_{10}$/IrMn/Cr(2/10/5/2 nm). Note that "//" indicates the position of the substrate. Electron-transparent windows were patterned into the back surface of the Si wafers using optical patterning and etching to make samples suitable for Lorentz transmission electron microscopy (TEM) (LTEM) studies. The growth conditions and seed layers were identical for samples with and without the IrMn, and the IrMn is grown on top of the ferromagnet to ensure that the microstructure of the ferromagnetic layer is the same.

Circular exchange bias coupling between the ferromagnetic and antiferromagnetic layers (i.e., imprinting the vortex state in the AF) was induced by cooling disks exhibiting a centered vortex magnetic configuration through the blocking temperature of IrMn (i.e., from 513 K) in zero external field. Note that since a large number of CoFe/IrMn disks exhibited domain walls in the as-deposited state, prior to the ZFC treatment the CoFe/IrMn sample was demagnetized in order to maximize the number of disks with the vortex magnetization state. For comparison, some samples were field cooled (FC) in a 5 kOe field through the blocking temperature to provide a uniform exchange bias.

LTEM experiments enable the magnetic contrast of the vortex to be visualized as a white or black dot. The dot is located at the vortex core position but the contrast is indicative of the vortex chirality, which can be determined uniquely from its magnetic contrast and the sign of the objective lens defocus (see, for example, Ref. 35). This method is insensitive to the state of the antiferromagnet, as it is a function only of the integrated magnetic induction through the sample. LTEM was performed on a FEI Tecnai F20ST operating at 200 kV. Vortices were swept out of the disks and renucleated by changing the intensity of a magnetic field applied *in situ* in the microscope. The field was applied by tilting the sample 30° around the holder axis and weakly exciting the objective lens. The field of the objective lens is along the electron-beam direction but the geometry of the tilted sample is such that there is an effective in-plane magnetic field. The direction of the applied field was reversed by reducing the objective lens excitation to zero, tilting the sample in the opposite direction (−30°), and exciting the objective lens again. The in-plane component of the remanent field in the objective lens at a 30° tilt was 66 Oe with the objective lens turned off. With the cautioning remark that the perpendicular component of this field may influence the behavior of small magnetic elements,[36] we observed that this field was not strong enough to modify the in-plane remanent magnetization states. The hysteresis loops were measured using a longitudinal MOKE setup capable of focusing the laser beam down to 3 $\mu$m with a maximum in-plane applied field of 1500 Oe.

Numerical simulations were based on integrating the Landau-Lifshitz-Gilbert (LLG) equation of motion for the magnetic moments. A simulation cell size of $2\times2\times2$ $nm^3$ was used for the exchange-biased bilayer disks. A grain structure with an average size of 20 nm was simulated by seeding random nucleation sites, which grew until their boundaries met. This grain structure was propagated conformally through the thickness of the IrMn and the Py and CoFe layers, respectively. The exchange bias coupling was modeled using an interfacial energy density acting on the FM surface in contact with the AF, which gives rise to an effective field $H_{EB}$. The AF itself was not simulated micromagnetically but only represented through this effective field. A circular exchange bias field was obtained in the following way. The FM magnetization was first relaxed into an equilibrium vortex state in zero external field and without an exchange bias interaction with the AF. The direction of $H_{EB}$ acting on the surface of each FM grain in contact with the AF was then taken as the in-plane average direction in each grain of the FM magnetization in the equilibrium vortex state adjacent to the AF. A uniaxial magnetocrystalline anisotropy was then added to the CoFe grains, with the axis within each FM grain set at a random in-plane direction and with all cells belonging to one grain having the same easy axis. For the single-layer Py and CoFe disks, the standard LLG micromagnetic simulator was used, with a cell size of 4 nm in plane and 12 nm out of plane.

## III. RESULTS

As an aid to understanding the behavior displayed by the vortex during the magnetization reversal process, Fig. 1 illustrates schematically an ideal vortex reversal mechanism in a single-layer FM disk with zero magnetocrystalline anisotropy. A vortex [Fig. 1(a)] displaces normal to the applied field toward either site A or site B in Fig. 1(b), such that the region of magnetization parallel to the field increases. If a field is applied as shown in Fig. 1(c), a vortex with counterclockwise (CCW) chirality is displaced toward site B. The vortex is then expelled from the lower edge of the disk, and the disk magnetization saturates to the left [Fig. 1(d)]. When the applied field is reduced from saturation, two mechanisms for vortex renucleation are possible. As illustrated in Fig. 1(e), for the "fixed chirality" mechanism the vortex nucleates at site B, which is the annihilation site of the previous vortex [Fig. 1(c)] with the same chirality (CCW, imaged white in LTEM). Thus, as the field is swept back and forward, the vortex contrast seen in the LTEM images is always white and the vortex nucleates alternately at sites A and B. For the "fixed nucleation site" mechanism, the vortex nucleates from site A, indicated by a black dashed circle in Fig. 1(f). For both directions of applied field the vortex nucleates at site A

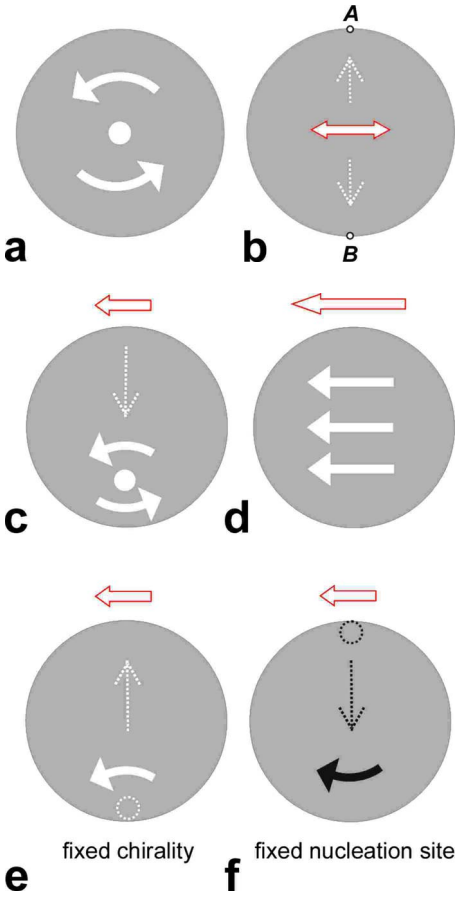


FIG. 1. (Color online) Schematic representation of vortex magnetization reversal in single-layer soft FM disks. Solid arrows indicate magnetization chirality inside the disk, hollow arrows indicate direction and magnitude of the applied field, and dotted arrows indicate direction of vortex motion. Letters A and B in (b) denote nucleation/annihilation sites. Dotted circle in (e) and (f) indicates the vortex nucleation site characteristic of the specific reversal mechanism (color matches the vortex chirality contrast seen in LTEM). Field sequence is (c) increasing field to the left, (d) saturating field to the left, followed by either (e) or (f) when decreasing the field again.

and is expelled at site B. Therefore its chirality *must* alternate with the direction in which the field increases. In this case the LTEM images would show the vortex chirality contrast alternating between white and black as the field saturates to the left and to the right. Analysis of these two mechanisms shows that the chirality, the direction of motion, and the vortex nucleation site are interdependent parameters. The choice of nucleation site (A or B) dictates the chirality and the direction of motion of the subsequently nucleating vortex, and similarly, the choice of chirality of the nucleating vortex determines its nucleation site and its direction of motion.

The single-layer Py disks spontaneously formed single vortices at remanence, with equal distribution of chiralities among the disks [50% clockwise (CW) and 50% counterclockwise chirality] as expected for a noninteracting array of disks.[37,38] The magnetization reversal proceeded via vortex nucleation and annihilation, with vortices following a path perpendicular to the direction of the in-plane field. The reversal process in the Py disks followed the fixed nucleation site mechanism [Fig. 1(f)] with the chirality alternating between CW and CCW. However, occasionally a nucleation event deviates to follow the fixed chirality mechanism. A real-time movie of 1 $\mu$m diameter Py disks in an alternating magnetic field of amplitude 283 Oe and frequency of 1 Hz can be seen in the supplementary material (Ref. 39). An example of this behavior is shown in Fig. 2 for a Py disk that initially exhibits white vortex chirality contrast [indicated by the solid white arrow in Fig. 2(a)]. The round white feature at the right side of the disk is not magnetic and appears unchanged in Figs. 2(a)–2(f). The disk appears oval due to the tilt around the holder axis employed to apply the in-plane field. The field was increased [Figs. 2(a) and 2(b)], saturated at 205 Oe, and then reduced to zero. The vortex nucleated from the expelling site [Fig. 2(c) with the same chirality (white)]. Upon increasing the field with opposite sign [Figs. 2(c) and 2(d)], saturating and decreasing the field, the vortex nucleated at the same site as in Fig. 2(c), but with opposite chirality shown by the black dot seen in Fig. 2(f). The mechanism described here is consistent with the statistical observations of chirality switching in submicron Py nanodisks of Schneider *et al.*[40] The occasional randomness in the nucleation mechanism can be attributed to edge roughness,[41] intrinsic microstructural variations,[42] and pinning[43] which can randomize the magnetization reversal process.

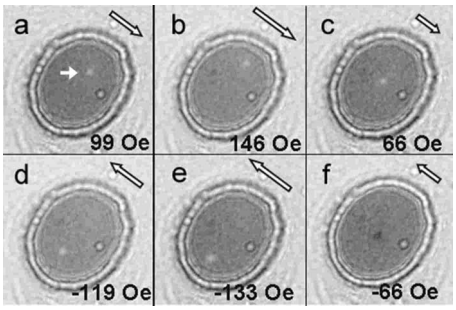


FIG. 2. Magnetization reversal in a 1 $\mu$m diameter Py disk with field applied *in situ* in the TEM. Open arrows indicate field direction and numbers indicate the in-plane field value. Images were obtained in the order shown with saturating fields applied between frames (b) and (c) and between (e) and (f). White arrow in (a) indicates position of vortex.

An important result of our work is that the magnetization reversal in ZFC exchange-biased Py/IrMn disks is markedly different from that of single-layer Py disks. It consistently follows the fixed chirality mechanism shown in Fig. 1(e) in which the vortex chirality is defined by the chirality *prior to the ZFC treatment*. The vortex nucleates alternately at A and B while cycling the field and maintains its chirality at each nucleation event, over an arbitrarily large number of field cycles. A movie of 1 $\mu$m diameter ZFC Py/IrMn disks in a magnetic field of amplitude 621 Oe and frequency of 1 Hz can be seen in the supplementary material (Ref. 39). The fact that the fixed chirality of the vortex is a consequence of the specific reversal mechanism imposed by the exchange bias and it does not occur in single-layer Py disks may seem surprising at first. Vortex chiralities in an as-prepared disk array are evenly distributed between CW and CCW, and the

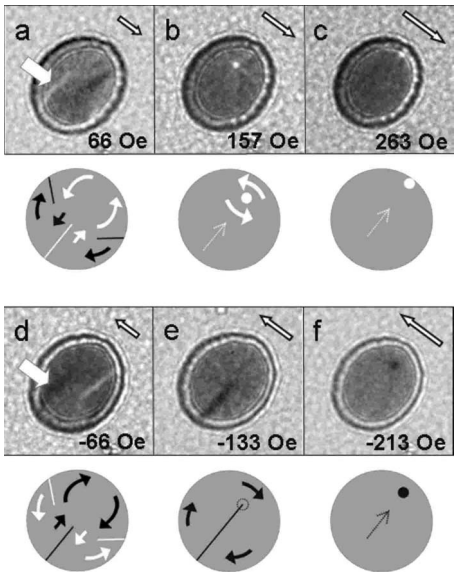


FIG. 3. LTEM images of ZFC CoFe/IrMn 1 $\mu$m diameter disks with field applied. Disks were brought in vortex state *in situ*, then cooled from 500 K prior to magnetizing. White arrows in (a) and (d) indicate the domain wall that will form the vortex in (b) and (f), respectively. Images were obtained in the order shown. The disks were saturated along the negative direction prior to (a) and in the positive direction prior to (d). Schematic under each LTEM image shows the corresponding magnetization state.

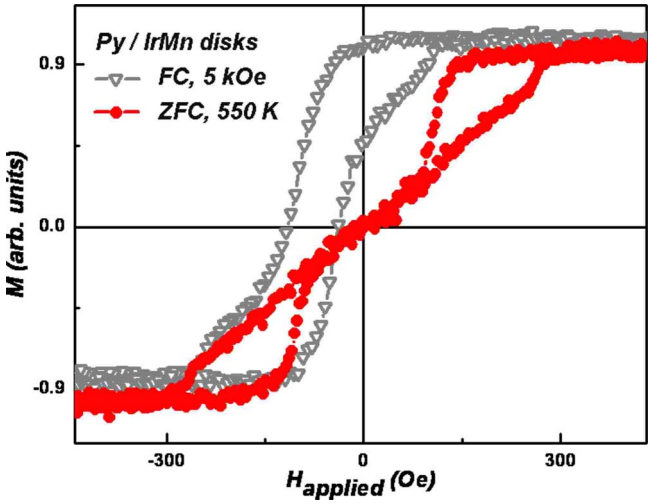


FIG. 4. (Color online) MOKE hysteresis loops for 1 $\mu$m diameter Py/IrMn disks, ZFC from 550 K (filled circles), and FC from 550 K in a 5 kOe field (open triangles).

only symmetry-breaking factors for the distribution of chiralities that have been reported to date make use of an asymmetry in the element shape or in the field.[8,9,13,15] Our Lorentz TEM observations indicate unequivocally that circular exchange bias imposes a single chirality in ZFC Py/IrMn disks. This is a process which can set a well-defined, unique chirality state in the FM vortex which is thermally stable and can be subsequently changed using, e.g., a magnetic field gradient[15] and an adequate thermomagnetic treatment.

CoFe and CoFe/IrMn disks most frequently obeyed a similar fixed nucleation site mechanism to that observed in the Py disks, with the difference that the vortex formation was preceded by the formation of a set of two or three domain walls, of which the central one determines the magnetic contrast of the vortex. In the ZFC CoFe/IrMn disk shown in Fig. 3 only two domain walls can be identified unequivocally during reversal, but the three-domain-wall configuration occurs frequently and it follows the same mechanism. For ease of understanding, the three-domain-wall configuration is chosen to illustrate schematically the reversal in Fig. 3: after saturating the initial vortex state at 442 Oe and reducing the field to remanence [Fig. 3(a)] the disk exhibited a set of domain walls. The white domain wall indicated by the thick arrow in Fig. 3(a) collapses into a white vortex [Fig. 3(b)] which is further displaced by the increasing field [Fig. 3(c)]. After saturation and removal of field, the same configuration of domain walls as in Fig. 3(a) appears [Fig. 3(d)], but with opposite contrast, as expected for the fixed nucleation site mechanism. Upon increasing the field in the opposite direction, the central black wall elongates [Fig. 3(e)] and the side wall(s) are expelled until the increase in magnetostatic energy favors the formation of a black vortex [Fig. 3(f)].

Reversal in single-layer CoFe disks is affected by random nucleation events in the same way as observed for the Py disks. A few CoFe disks exhibited reversal paths consisting of distinct combinations of domain walls, multiple vortices, or vortices coexisting with domain walls. Unlike in Py disks however, in CoFe disks randomness in reversal can occur both in the time domain (the same disk may reverse differently over time) and in the spatial domain (different disks may reverse differently during the same magnetization cycle). However, following ZFC, reversal randomness occurring in the time domain was removed for the CoFe/IrMn disks and the magnetization predictably followed the mechanism described in Fig. 3 for any number of magnetization cycles. This observation can have important practical applications, as either of the two chiralities of the vortex can be accessed by simply cycling the field.

Hysteresis loops measured using MOKE magnetometry are shown in Fig. 4 for Py/IrMn disks and in Fig. 5 for CoFe/IrMn disks. Large open circles labeled (a)–(f) in Fig. 5 correspond approximately to the field points at which the LTEM images in Fig. 3 were recorded. The coercivity and loop shift of Py/IrMn and CoFe/IrMn disks in FC and ZFC states are listed in Table I, where the field was applied along the direction of field cooling for the FC measurements. The hysteresis loop of the Py/IrMn ZFC disks exhibits zero coercivity, no loop shift, and a central portion of reversible magnetization over the range of approximately −125–+125 Oe. The corresponding FC loop exhibits a finite coercivity and loop shift as expected. For the ZFC CoFe/IrMn disks, a constricted loop with a negligible loop shift is observed. As a result of nonzero magnetocrystalline anisotropy of CoFe, the central part of the ZFC CoFe/IrMn disks loop is not reversible but has a finite coercivity, albeit smaller than that of the FC loop. Note that the FC loop for CoFe/IrMn does not show reversal by vortex formation.

LTEM shows that at zero applied field the vortices are centered on the disks in Py and Py/IrMn, regardless of the

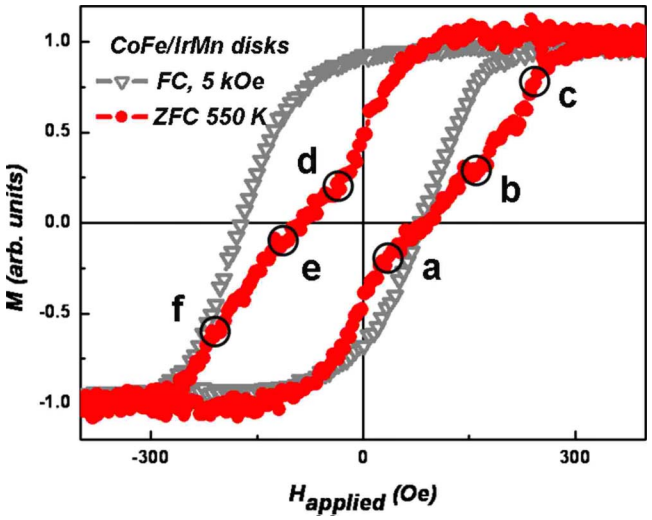


FIG. 5. (Color online) MOKE hysteresis loops for 1 $\mu$m diameter CoFe/IrMn disks, ZFC from 550 K (filled circles), and FC from 550 K in a 5 kOe field (open triangles).

magnetic history of the samples, which is consistent with the hysteresis curve of ZFC Py/IrMn disks having a reversible central portion passing through origin (see Fig. 4). In contrast, at zero applied field, vortices of opposite chiralities in both CoFe and ZFC CoFe/IrMn disks are slightly displaced from the center of the disks in opposite directions, depending on the magnetic history of the sample, which is consistent with the finite coercivity of the ZFC hysteresis loop in Fig. 5.

The displacement $d$ of the vortex core from the center of the disks is plotted as a function of the *in situ* applied field in Fig. 6 for Py and ZFC Py/IrMn disks and in Fig. 7 for CoFe and ZFC CoFe/IrMn disks. Filled circles indicate experimental data, and empty circles indicate micromagnetic simulations. The inset of Fig. 6(a) shows that the displacement averaged for four disks in two consecutive magnetization

TABLE I. Coercivity and exchange bias for the bilayers subjected to two different thermomagnetic treatments (FC and ZFC). $H_{EB}^{ZFC}$ is the effective exchange bias field obtained from simulations. The coercivities of the corresponding continuous films are $H_C^{CoFe,film}=37.5$ Oe and $H_C^{Py,film}\sim 0$ Oe.

| | | $H_C$ (Oe) | Loop shift $H_{EB}$ (Oe) | $H_{EB}^{ZFC}$ (Oe) |
|---|---|---|---|---|
| Py/IrMn | ZFC | 0 | 0 | 104 |
| | FC | 40 | 78 | |
| CoFe/IrMn | ZFC | 88 | 5 | 174 |
| | FC | 127 | 46 | |

experiments is representative of the ensemble; all experimental data presented are therefore averages of four disks. The vortex motion in the ZFC bilayer disk is subject to strong local pinning such that upon a very slow increase in the applied field (at a rate of $\sim 5$ Oe/s) the vortex executes four to six discrete "jumps" across the diameter of the disk before annihilating. The pinned motion can also be observed in the single-layer disks but with much lower strength and with a more finely spaced distribution of pinning sites. Moreover, it can be seen that the slope of the vortex displacement for the single Py disks is somewhat larger than for the Py/IrMn disks. Micromagnetic simulations for several values of the exchange bias field are plotted in the inset of Fig. 6(b).

The simulations in the inset of Fig. 6(b) show that a larger exchange bias field stiffens the confining potential of the vortex, such that a larger field is necessary for a given vortex displacement. The simulated curves with $H_{EB}=104$ Oe and $H_{EB}=174$ Oe give the best fit to the experimental curve for the ZFC Py/IrMn and CoFe/IrMn disks, respectively. A variation from 0 to 130 Oe of the magnetocrystalline anisotropy field for CoFe (not shown) did not significantly alter the shape of the vortex displacement versus field plot. The values of the exchange bias field $H_{EB}^{ZFC}$ obtained from fitting the

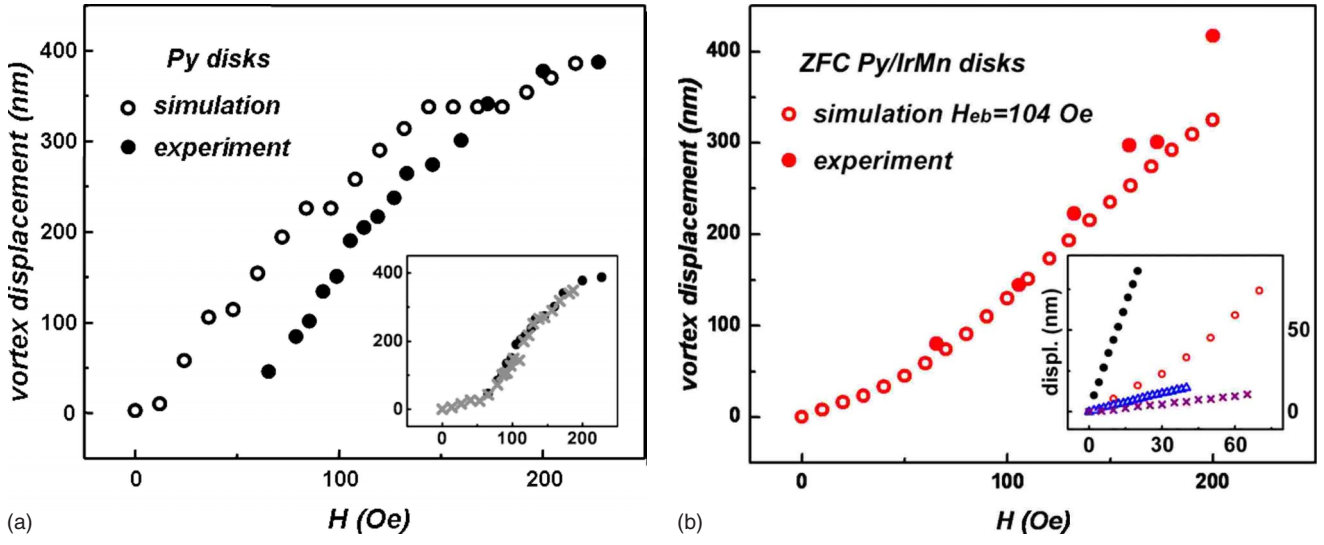


FIG. 6. (Color online) Displacement of vortex vs applied field in (a) Py and relative displacement in (b) ZFC Py/IrMn 1 $\mu$m diameter disks. Inset of (a) shows results of two consecutive magnetization experiments. Inset of (b) shows vortex displacement obtained from micromagnetic simulations with $H_{EB}$ values of 0, 104, 208, and 416 Oe, respectively, in the order of decreasing slope.

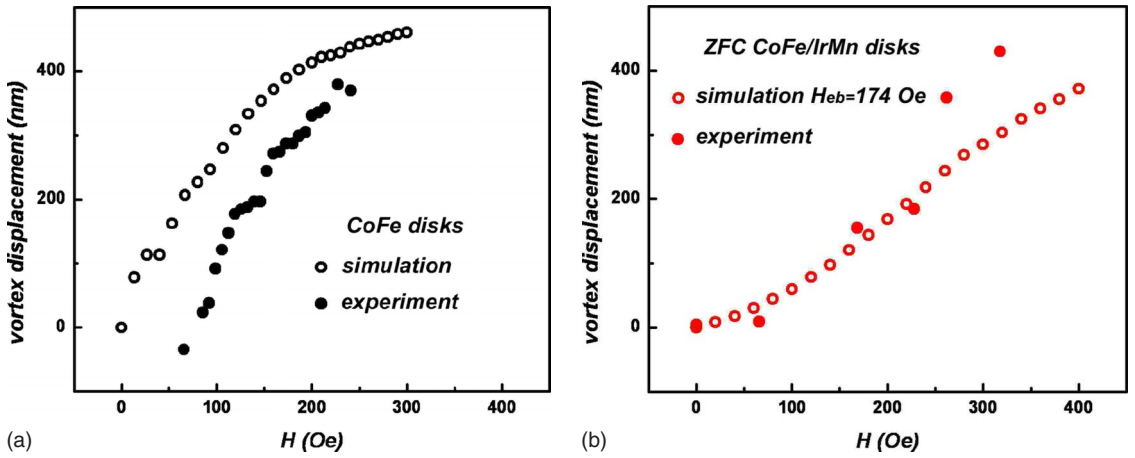


FIG. 7. (Color online) Displacement of vortex vs applied field in (a) CoFe and relative displacement in (b) ZFC CoFe/IrMn 1 $\mu$m diameter disks.

numerical simulations to the experimentally observed vortex displacement differ from the values of $H_{EB}$ obtained from the FC loop shifts, especially for CoFe/IrMn. There are several possible reasons for this. First, we note that the steeper rise in core displacement for fields larger than 200 Oe in Fig. 7(b) may indicate a slightly lower exchange bias than obtained from matching only the first four points in the figure. More importantly, there is no fundamental reason that the field obtained from the loop shift should be identical to that obtained from the core displacement. It has been shown previously[32] that circular exchange bias leads to an additional parabolic confinement potential of the vortex core (in addition to the one resulting from magnetostatic fields). Core displacements measured in minor loops should therefore be correlated with this confining potential and be largely reversible, with only minor dissipative processes stemming from random pinning sites and local variations in magnetocrystalline anisotropy. In contrast, the loop shift involves a convolution of exchange bias with rather significant dissipative processes.

## IV. DISCUSSION

For the Py and ZFC Py/IrMn disks the magnetization reversal has a reversible central portion, there is no hysteresis loop shift, and the reversal is symmetric about the origin which results in zero coercivity. Both LTEM and MOKE observations are consistent with an exchange bias field with circular geometry and a unidirectional character giving rise to a well-defined chirality rather than the unidirectional configuration that results from the FC treatment.

In order to understand the effect that "circular" exchange bias has on the magnetization reversal of the bilayer disks, a closer look at the reversal of the single-layer FM disks is necessary. The fixed chirality and fixed nucleation site reversal paths shown in Fig. 1 have the same energy, and therefore they have the same probability to be chosen during reversal. However, the consistent choice of the fixed nucleation site reversal mechanism in the Py disks leads us to believe that microstructure plays an important role in symmetry breaking, such that the vortex nucleation energy at one of the two possible nucleation sites [A or B in Fig. 1(c)] is lower. On the other hand, reversal in the ZFC Py/IrMn disks occurs preferentially via the fixed chirality mechanism. In this case, the symmetry-breaking factor is the circular exchange bias which imprints a defined chirality into the antiferromagnet and leads to this chirality having a lower energy than the opposite chirality and thus to a reversal mechanism in which that same chirality is preferred. This chirality is determined by the chirality of the FM vortex prior to the zero-field cooling treatment. The alternating chirality of the vortices observed in Py disks and the alternating nucleation sites in ZFC Py/IrMn disks are thus consequences of the particular mechanism of reversal governed either by microstructure or by exchange bias.

A similar analysis suggests that microstructure is the leading factor controlling the reversal of CoFe disks, which occurs via the fixed nucleation site mechanism. In this case reversal is via formation of domain walls at the fixed nucleation site, followed by collapse to form a vortex. We would expect reversal in ZFC CoFe/IrMn disks to be dominated by exchange bias as for the ZFC Py/IrMn disks. However the reversal mechanism is identical to that of single-layer CoFe disks, which leads us to believe that exchange bias, although stronger than in Py/IrMn disks, is not the leading term in the energy balance of the nucleating vortex.

However, as in the Py/IrMn, in CoFe/IrMn one of the effects of exchange bias is to counteract thermal activation effects in the ferromagnet (Ref. 44) and impose a single magnetization reversal path over time. Following the ZFC treatment, reversal is reproducible over an indefinite number of magnetization cycles for both Py/IrMn and CoFe/IrMn disks. It is worth noting that the suppression of the stochastic character typical of vortex reversal behavior by circular exchange bias may have interesting consequences, in particular for memory applications when it is necessary to have a well-defined magnetic state after a given magnetic history.

In addition, in Py/IrMn disks the circular exchange bias causes reversibility in the vortex motion along any in-plane direction, for a range of fields centered about zero. In this field region the vortex exists in all four quadrants of the

hysteresis loop and its position depends on the value of the field, but it does not depend on the field history. Reversibility manifests itself by equal displacements of the vortex upon application of equal and opposite fields in LTEM and in zero coercivity and a reversible central part of the MOKE loop. We can understand why circular exchange bias cause reversibility in ZFC Py/IrMn disks by noting that, as a result of the zero-field cooling treatment, the magnetization configuration imprinted as exchange bias in the AF reproduces the lowest-energy state of the FM vortex. This is obtained by allowing the FM vortex to reach its equilibrium state at the annealing temperature, in the absence of exchange bias. After cooling at room temperature, reversal in FM/AF bilayer disks follows an energy path dictated by the imprinted vortex state in the AF vortex. Since this is the lowest-energy path the FM vortex can follow during its reversal and we know that thermal effects are suppressed, the vortex motion is reversible in the field range in which the vortex exists in all four quadrants of the loop. Since approximately 80 disks contribute to signal in each MOKE curve, the behavior we described is an average over all disks and slight individual deviations from this behavior may exist. For ZFC CoFe/IrMn disks, a minimum-energy path is still accessible but through a different reversal mechanism. This mechanism involves nucleating and moving domain walls in a medium with finite magnetocrystalline anisotropy and therefore produces hysteresis in reversal and consequently a finite loop width as seen in MOKE. However, in CoFe/IrMn either (i) the imprinted vortex state in the AF is inhomogeneous, leading to a complex reversal or (ii) although the imprinted state in the AF was a perfect vortex, CoFe disks for the studied thickness and diameter are at the border between vortex reversal and multidomain reversal and the energy of the AF is not sufficient to drive the reversal toward a pure vortex reversal. Note that even for minor hysteresis loops in which the vortex is not expelled and reversal is therefore only via vortex motion, the reversal behavior is still hysteretic as a result of the presence of a combination of magnetocrystalline anisotropy, microstructural pinning sites, and the presence of exchange bias.

The vortex-mediated reversal mechanism indicates that demagnetization energy plays an important role in the magnetic energy balance of the disks. As a result of the negligible magnetocrystalline anisotropy of Py, reversal of the magnetization in Py and ZFC Py/IrMn micron-sized disks takes place solely via vortex formation and annihilation.[1] The more complex reversal mechanism observed in CoFe and ZFC CoFe/IrMn disks, involving both vortices and domain walls, suggests a competition between the demagnetization and anisotropy energy terms. The hysteresis loops of all but the FC CoFe/IrMn sample are characteristic of vortex-mediated reversal, indicating that the predominant remanent states are flux closure (vortex) states. Since the hysteresis curve for the CoFe/IrMn disks acquires the features characteristic of vortex reversal following the ZFC treatment, we believe that demagnetization above the blocking temperature and the ZFC treatment, leading to the formation of a circular exchange bias state, favor vortex reversal as the dominant mechanism by stabilizing the vortex state at the expense of domain wall-containing "*S*" states.[26,45] In both Py/IrMn and CoFe/IrMn disks the stabilization of the vortex state produced by circular exchange bias is manifested in an increase in $H_n$ and $H_a$, as compared with the as-deposited state.

The increase in annihilation fields and the decreased slope of the vortex displacement versus applied field curves upon ZFC indicate that the circular exchange bias stabilizes the vortex configuration in the FM layer. The decreased slope was observed in both micromagnetic simulations [see inset of Fig. 6(b) for Py/IrMn] and experimentally for both Py/IrMn and CoFe/IrMn ZFC disks [see Figs. 6(b) and 7(b)]. The stabilization of the vortex upon ZFC can be understood assuming that the ZFC treatment sets the exchange bias in the geometry of the ferromagnetic vortex field centered in the disk. The exchange coupling field acts to keep the interfacial FM and AF moments parallel, whereas the external field acts to displace the FM moments collectively as a vortex, creating a torque on the FM moments not situated along the vortex displacement direction. The net result of individual microscopic torques is a restoring force acting toward the equilibrium centered position, such that the displacement of a ZFC vortex requires a larger applied field than the same displacement of a single-layer FM vortex.

In CoFe/IrMn disks, vortices exhibit small, randomly oriented displacements from the center of the disk in the absence of an external field. After magnetization and removal of the field, the small displacements are oriented along a direction perpendicular to the last applied field. The displacements of vortices with opposite chiralities have opposite signs along this direction, which is consistent with the finite coercivity of the ZFC hysteresis loop in Fig. 5. The finite vortex displacement in zero field is present in CoFe disks as well which may be caused by pinning by defects such as grain boundaries or variations in the orientation of the local anisotropy axes. In-plane angle invariance of the magnetization reversal and the symmetry about zero applied field indicate that the magnetic behavior of both Py and CoFe layers in the ZFC AF/FM disks acquires the same circular symmetry as the exchange bias interaction.

The ZFC treatment is not expected to produce a macroscopic hysteresis loop shift due to the circular symmetry of the exchange bias. In the absence of shift, we estimated the strength of circular EB ($H_{\mathrm{EB}}^{\mathrm{ZFC}}$) in two different ways. Sort *et al.*[30] observed that the FC loop shift $H_{\mathrm{EB}}$ is equal to the increase in annihilation fields from the single layer to the ZFC state, $\Delta H_a = H_a^{\mathrm{ZFC}} - H_a^0$, where $H_a$ is the annihilation field and the superscripts refer to the ZFC state and the single-layer disks, respectively. Correcting for the FC loop shift, $H_a^0$ and $H_a^{\mathrm{FC}}$ are approximately equal, and we can write $H_{\mathrm{EB}}^{\mathrm{ZFC}} = H_a^{\mathrm{ZFC}} - H_a^{\mathrm{FC}}$. We observe the same effect in our ZFC Py/IrMn disks for which $\Delta H_{a1} = 82$ Oe and $\Delta H_{a2} = -87$ Oe for the two branches of the ZFC MOKE loop, very close to $H_{\mathrm{EB}} = 78$ Oe, as measured from Fig. 4. This suggests that the strength of circular exchange bias is comparable to that of conventional exchange bias. However, the above reasoning cannot be used to estimate $H_{\mathrm{EB}}^{\mathrm{ZFC}}$ of CoFe/IrMn disks. From Table I the exchange bias field obtained from simulations is $H_{\mathrm{EB}}^{\mathrm{ZFC}} = 104$ Oe for ZFC Py/IrMn disks and $H_{\mathrm{EB}}^{\mathrm{ZFC}} = 174$ Oe for ZFC CoFe/IrMn disks, both larger than the corresponding loop shifts of 78 and 46 Oe for FC Py/IrMn and CoFe/IrMn disks, respectively. The discrepancy between the ZFC and

FC values is significantly larger in CoFe/IrMn than in Py/IrMn. There are different possible explanations for this behavior. First, it has to be taken into account that the imprinted state in the AF in the case of CoFe may not be a homogeneous vortex state. Another factor to be taken into account when comparing micromagnetic simulations with experimental data is that in the simulations data are obtained from a single disk in vortex state at remanence, whereas the MOKE curve is an average signal of about 80 disks, which have been shown by LTEM to exhibit different magnetization reversal modes. Most importantly, the macroscopic $H_{EB}$ might depend on the reversal mode such that $H_{EB}$ obtained from a FC treatment, which results in domain-wall reversal, cannot be compared with $\Delta H_a$ obtained from a ZFC treatment, which results in domain wall+vortex reversal. Dynamic effects related to the speed of reversal may also play a role since the field is cycled with about 15 ms/loop in MOKE and quasistatically in LTEM.

## V. CONCLUSIONS

In this work we have investigated the magnetization reversal behavior of FM disks subjected to exchange bias with circular geometry. The vortex reversal mechanism in Py/IrMn disks changes from being microstructure-governed to exchange bias-governed upon the ZFC treatment and the reversal occurs with fixed chirality. The vortex state is stabilized against external fields, thermal effects are removed, and reversal becomes reproducible over time. The ZFC Py/IrMn and CoFe/IrMn exhibit constricted hysteresis loops with no loop shift. However, while Py/IrMn exhibit a reversible central part of the loop (i.e., perfect vortex reversal), CoFe/IrMn has a finite coercivity, as the magnetization reversal involves domain walls. In this case the reversal does not acquire a fixed chirality but remains qualitatively identical to that of CoFe disks, showing that the magnetization reversal is governed not only by the exchange bias but also by anisotropy and its local variations.

## ACKNOWLEDGMENTS

This work was carried out in part at UChicago Argonne, LLC, operator of Argonne National Laboratory. Argonne, a U.S. Department of Energy Office of Science Laboratory, is operated under Contract No. DE-AC02-06CH11357. Use of the Center for Nanoscale Materials and of the Electron Microscopy Center of Argonne National Laboratory is gratefully acknowledged. Partial financial support from the Spanish CICYT (Contract No. MAT2007-66302-C02), the Catalan DGR (Contract No. 2005-SGR-00401), and the Institut Català de Nanotecnologia is also acknowledged.

*Present address: Colorado State University, Fort Collins, CO 80523, USA.

[1] R. P. Cowburn, D. K. Koltsov, A. O. Adeyeye, M. E. Welland, and D. M. Tricker, Phys. Rev. Lett. **83**, 1042 (1999).
[2] B. D. Terris and T. Thomson, J. Phys. D **38**, R199 (2005).
[3] J. G. Zhu, Y. F. Zheng, and G. A. Prinz, J. Appl. Phys. **87**, 6668 (2000).
[4] J. Åkerman, Science **308**, 508 (2005).
[5] D. A. Allwood, G. Xiong, C. C. Faulkner, D. Atkinson, D. Petit, and R. P. Cowburn, Science **309**, 1688 (2005).
[6] T. Shinjo, T. Okuno, R. Hassdorf, K. Shigeto, and T. Ono, Science **289**, 930 (2000).
[7] K. Y. Guslienko, J. Nanosci. Nanotechnol. **8**, 2745 (2008).
[8] M. Schneider, H. Hoffmann, and J. Zweck, Appl. Phys. Lett. **79**, 3113 (2001).
[9] T. Taniuchi, M. Oshima, H. Akinaga, and K. Ono, J. Appl. Phys. **97**, 10J904 (2005).
[10] F. Giesen, J. Podbielski, B. Botters, and D. Grundler, Phys. Rev. B **75**, 184428 (2007).
[11] P. Vavassori, R. Bovolenta, V. Metlushko, and B. Ilic, J. Appl. Phys. **99**, 053902 (2006).
[12] K.-M. Wu, J.-F. Wang, Y.-H. Wu, C.-M. Lee, J.-C. Wu, and L. Horng, J. Appl. Phys. **103**, 07F314 (2008).
[13] V. L. Mironov, B. A. Gribkov, A. A. Fraerman, S. A. Gusev, S. N. Vdovichev, I. R. Karetnikova, I. M. Nefedov, and I. A. Shereshevsky, J. Magn. Magn. Mater. **312**, 153 (2007).
[14] Y. Gaididei, D. D. Sheka, and F. G. Mertens, Appl. Phys. Lett. **92**, 012503 (2008).
[15] M. Konoto, T. Yamada, K. Koike, H. Akoh, T. Arima, and Y. Tokura, J. Appl. Phys. **103**, 023904 (2008).
[16] M. Klaui, J. Rothman, L. Lopez-Diaz, C. A. F. Vaz, J. A. C. Bland, and Z. Cui, Appl. Phys. Lett. **78**, 3268 (2001).
[17] J. Sort, K. S. Buchanan, J. E. Pearson, A. Hoffmann, E. Menéndez, G. Salazar-Alvarez, M. D. Baró, M. Miron, B. Rodmacq, B. Dieny, and J. Nogués, J. Appl. Phys. **103**, 07C109 (2008).
[18] W. Jung, F. J. Castano, and C. A. Ross, Phys. Rev. Lett. **97**, 247209 (2006).
[19] T. Yang, A. Hirohata, M. Hara, T. Kimura, and Y. Otani, Appl. Phys. Lett. **90**, 092505 (2007).
[20] B. C. Choi, J. Rudge, E. Girgis, J. Kolthammer, Y. K. Hong, and A. Lyle, Appl. Phys. Lett. **91**, 022501 (2007).
[21] W. H. Meiklejohn and C. P. Bean, IEEE Trans. Magn. **37**, 3866 (2001).
[22] K. Li, Y. Wu, Z. Guo, Y. Zheng, G. Han, J. Qiu, L. An, and T. Zhou, J. Nanosci. Nanotechnol. **7**, 13 (2007).
[23] J. Nogues and I. K. Schuller, J. Magn. Magn. Mater. **192**, 203 (1999).
[24] R. L. Stamps, J. Phys. D **33**, R247 (2000).
[25] J. Nogués, J. Sort, V. Langlais, V. Skumryev, S. Surinach, J. S. Munoz, and M. D. Baró, Phys. Rep. **422**, 65 (2005).
[26] J. Sort, A. Hoffmann, S. H. Chung, K. S. Buchanan, M. Grimsditch, M. D. Baró, B. Dieny, and J. Nogués, Phys. Rev. Lett. **95**, 067201 (2005).
[27] Z. P. Li, O. Petracic, J. Eisenmenger, and I. K. Schuller, Appl. Phys. Lett. **86**, 072501 (2005).
[28] A. Hoffmann, J. Sort, K. S. Buchanan, and J. Nogués, IEEE Trans. Magn. **44**, 1968 (2008).
[29] R. Nakatani, T. Yoshida, Y. Endo, Y. Kawamura, M. Yamamoto,

T. Takenaga, S. Aya, T. Kuirowa, S. Beysen, and H. Hobayashi, J. Magn. Magn. Mater. **286**, 31 (2005).
[30] J. Sort, G. Salazar-Alvarez, M. D. Baro, B. Dieny, A. Hoffmann, V. Novosad, and J. Nogués, Appl. Phys. Lett. **88**, 042502 (2006).
[31] J. Sort, K. S. Buchanan, V. Novosad, A. Hoffmann, G. Salazar-Alvarez, A. Bollero, M. D. Baró, B. Dieny, and J. Nogués, Phys. Rev. Lett. **97**, 067201 (2006).
[32] O. G. Heinonen, D. K. Schreiber, and A. K. Petford-Long, Phys. Rev. B **76**, 144407 (2007).
[33] R. D. Gomez, T. V. Luu, A. O. Pak, K. J. Kirk, and J. N. Chapman, J. Appl. Phys. **85**, 6163 (1999).
[34] J. Raabe, R. Pulwey, R. Sattler, T. Schweinbock, J. Zweck, and D. Weiss, J. Appl. Phys. **88**, 4437 (2000).
[35] X. Portier and A. K. Petford-Long, J. Phys. D **32**, R89 (1999).
[36] R. E. Dunin-Borkowski, M. R. McCartney, B. Kardynal, D. J. Smith, and M. R. Scheinfein, Appl. Phys. Lett. **75**, 2641 (1999).
[37] V. Novosad, K. Y. Guslienko, H. Shima, Y. Otani, S. G. Kim, K. Fukamichi, N. Kikuchi, O. Kitakami, and Y. Shimada, Phys. Rev. B **65**, 060402(R) (2002).
[38] M. Natali, A. Popa, U. Ebels, Y. Chen, S. Li, and M. E. Welland, J. Appl. Phys. **96**, 4334 (2004).
[39] See EPAPS Document No. E-PRBMDO-79-038901 for supplementary movies. For more information on EPAPS, see http://www.aip.org/pubservs/epaps.html.
[40] M. Schneider, H. Hoffmann, and J. Zweck, Appl. Phys. Lett. **77**, 2909 (2000).
[41] J. W. Lau, R. D. McMichael, M. A. Schofield, and Y. Zhu, J. Appl. Phys. **102**, 023916 (2007).
[42] A. Fernandez and C. J. Cerjan, J. Appl. Phys. **87**, 1395 (2000).
[43] R. L. Compton and P. A. Crowell, Phys. Rev. Lett. **97**, 137202 (2006).
[44] Y. G. Wang and A. K. Petford-Long, J. Appl. Phys. **92**, 6699 (2002).
[45] M. Schneider, H. Hoffmann, S. Otto, T. Haug, and J. Zweck, J. Appl. Phys. **92**, 1466 (2002).